A Local Excitation and Measurement Approach for Decentralized Damage Detection using Transmissibility Functions

Dapeng Zhu, Xiaohua Yi, Yang Wang*
School of Civil and Environmental Engineering
Georgia Institute of Technology
Atlanta, GA 30332, USA

ABSTRACT

In order to assess structural safety conditions, many vibration-based damage detection methods have been developed in recent years. Among these methods, transmissibility function analysis can offer advantages in easy and low-cost implementation, as well as independency to the magnitude and waveform of an excitation record. Harnessing these features, a decentralized structural damage detection procedure is proposed in this paper. The proposed procedure only requires measurements in one small area at a time, and thus, is ideal for using limited number of sensors upon a large scale structure. This study also investigates the nature of transmissibility functions for damage detection in an analytical manner, based on a chain-like spring-mass-damper system with multiple degrees-of-freedom (DOFs). The analytical derivation is validated through numerical simulation and laboratory experiments using mobile sensors.

Keywords: Transmissibility function, damage detection, decentralized approach, local excitation and measurement, mobile sensors

1. INTRODUCTION

Large-scale civil structures, such as bridges, dams, and high-rise buildings may experience harsh operational environment or severe natural disasters during their lifespan. Taking bridges as an example, more than one in nine of the bridges in the United States were categorized as structurally deficient, according to the 2013 ASCE Report Card for America's Infrastructure[1]. It was estimated that a $20.5 billion annual investment is needed to substantially improve the bridge conditions, yet currently, only $12.8 billion is spent annually on the construction and maintenance of bridges. In order to efficiently utilize the limited resources and prioritize retrofit tasks, reliable evaluation of structural conditions is essential. Over the past few decades, structural health monitoring (SHM) systems have been widely studied for assessing the condition of large-scale civil structures [2, 3]. In an SHM system, various types of sensors, such as accelerometers, stain gauges, thermometers, displacement and velocity transducers, can be used for monitoring structural behavior. A data acquisition (DAQ) system usually collects all the sensor measurements at a central server. However, the SHM system still suffers from high cost. For example, the cost of installing a typical structural monitoring system in a mid-rise building can exceed a few thousand dollars per sensing channel [4]. To overcome the difficulty, decentralized SHM approaches can be explored. In contrast to centralized approaches that operate on an entire structure model and require data from the entire structure, a decentralized approach only requires a limited number of sensing channels, operates on a local part of a structure, and mainly requires local structural response data.

In recent years, significant research efforts have been devoted to various structural damage detection techniques[5, 6]. Most of the techniques can be categorized as two groups. The first category contains local approaches, such as acoustic emission [7], laser image [8], radar image [9], and impact-echo [10], etc. These approaches are applied mainly to detect local structural defect, such as cracks and corrosion. The second category contains global approaches, which has been mainly applied with structural vibration data. The approaches are based on the assumption that damage induces changes in structural mass, damping, or stiffness. Such changes cause detectable variations in structure dynamic properties, such as frequency response functions, vibration modal properties, etc. For example, comprehensive reviews on vibration-based damage identification algorithms can be found in [5] and [6]. Nevertheless, very few studies have investigated decentralized structural damage detection. One such example is [11], where frequency response functions are adopted to locate substructure damage on building structures under earthquake excitation. Measurement of the excitation is required for

* yang.wang@ce.gatech.edu; phone 1 404 894-1851; fax 1 404 385-0337; http://wang.ce.gatech.edu

calculating frequency response functions. Another example is a decentralized blind source separation algorithm proposed to use only a few sensor measurements at a time for system identification when disturbances contain narrowband frequencies [12].

Among vibration-based damage identification approaches, transmissibility function analysis attracts considerable interest due to its simple and low-cost implementation, effectiveness in damage identification, and independency to the magnitude and waveform of the excitation records. Harnessing these features, transmissibility functions can be exploited for decentralized structural damage detection without measurement of dynamic excitations. A number of researchers investigated the application of transmissibility function analysis for damage detection. For example, Zhang *et al.* studied the performance of transmissibility functions for damage detection within various frequency ranges through a laboratory experiment[13]. In the experiment, a piezoceramic patch actuator was used to excite a cantilever beam; translational and curvature transmissibility functions were adopted to calculate damage indicators and successfully locate damage. Kess and Adams analyzed the effects of operational and environmental variability on the transmissibility function analysis for damage detection on a woven composite plate[14]. Their work suggested that the damage detection accuracy based on transmissibility function could be improved by identifying specific frequency ranges that are more sensitive to damage and immune to sources of uncertainties. Devriendt and Guillaume [15] concluded that arbitrary forces could be used to perform the transmissibility-function-based operational modal analysis, as long as the structure is persistently excited in the frequency range of interest. Mao and Todd analyzed the uncertainty of the magnitude of transmissibility functions under random excitation[16]. The probability density of transmissibility functions are analytically derived and validated through Monte Carlo simulation. Finally, Johnson and Adams investigated the explicit formulation of transmissibility functions using a three degrees-of-freedom (DOFs) system [17]. Nevertheless, little research has been reported on decentralized damage detection using transmissibility function analysis. Furthermore, analytical nature of transmissibility functions for damage detection of a chain-like structure with an arbitrary number of DOFs is not available in the literature.

This study proposes a decentralized structural damage detection procedure. The decentralized procedure only requires measurements in one small area at a time, and thus, is ideal for using a limited number of sensors upon a large scale structure. Furthermore, this study investigates the nature of the transmissibility functions for decentralized damage detection in an analytical manner, using a chain-like multi-DOF spring-mass-damper system. The system used in the derivation is lightly coupled since each DOF is only connected with its neighboring DOFs on the chain. Damage sensitivity of the transmissibility functions is derived based on a decentralized measurement scheme. Responses at two neighboring DOFs are measured at a time, following the sequence 1 and 2, 2 and 3, etc., to cover the entire structure. To generate response at the two DOFs, external excitation is applied at the latter DOF in the pair. The analytical derivation is then validated through both numerical simulations and laboratory experiments. Section 2 of this paper presents an analytical derivation for the damage sensitivity of the decentralized/local transmissibility functions, which illustrates the potential of using change in local transmissibility functions as damage signatures. Two types of damage scenarios are studied. The first scenario considers mass change, and the second scenario considers stiffness loss. Section 3 presents the numerical simulation of a 10-DOF spring-mass-damper system that validates the conclusion from the analytical derivation. Section 4 presents the experimental validation using wireless mobile sensors on a five-story shear-building model. Section 5 summarizes this paper and discusses future research work.

2. TRANSMISSIBILITY FUNCTION ANALYSIS FOR A MULTI-DOF SPRING-MASS-DAMPER SYSTEM

In this section, the local transmissibility function for a multi-DOF spring-mass-damper system is first analytically derived, following a decentralized excitation and measurement scheme. The sensitivity of the transfer function for two damage scenarios is then studied. The first damage scenario considers mass change, and the second damage scenario considers stiffness loss.

2.1 Transmissibility function for a multi-DOF spring-mass-damper system

The equations of motion for a multi-DOF spring-mass-damper system can be formulated as:

$$\mathbf{M}\ddot{\mathbf{x}}(t) + \mathbf{C}\dot{\mathbf{x}}(t) + \mathbf{K}\mathbf{x}(t) = \mathbf{f}(t) \tag{1}$$

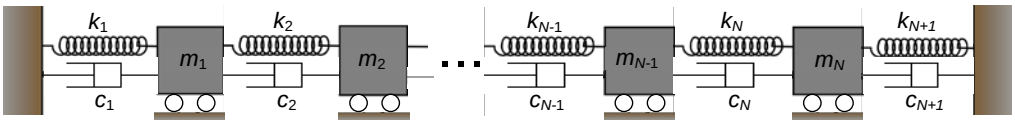

Figure 1. A chain-like multi-DOF spring-mass-damper system

where $\mathbf{x}(t)$, $\dot{\mathbf{x}}(t)$ and $\ddot{\mathbf{x}}(t)$ denote the displacement, velocity and acceleration vectors of the system, respectively; $\mathbf{f}(t)$ denotes the external excitation; **M**, **C,** and **K** are the mass, damping and stiffness matrices, respectively. For a chain-like spring-mass-damper system (Figure 1), the matrices can be expressed as the follows:

$$\mathbf{M} = \mathrm{Diag}\{m_1, m_2, \cdots, m_N\} \tag{2}$$

$$\mathbf{K} = \begin{bmatrix} k_1+k_2 & -k_2 & 0 & 0 & \cdots & 0 \\ & k_2+k_3 & -k_3 & 0 & \cdots & 0 \\ & & \ddots & \ddots & \ddots & \vdots \\ & & & k_{N-2}+k_{N-1} & -k_{N-1} & 0 \\ & \text{Symm.} & & & k_{N-1}+k_N & -k_N \\ & & & & & k_N+k_{N+1} \end{bmatrix} \tag{3}$$

$$\mathbf{C} = \begin{bmatrix} c_1+c_2 & -c_2 & 0 & 0 & \cdots & 0 \\ & c_2+c_3 & -c_3 & 0 & \cdots & 0 \\ & & \ddots & \ddots & \ddots & \vdots \\ & & & c_{N-2}+c_{N-1} & -c_{N-1} & 0 \\ & \text{Symm.} & & & c_{N-1}+c_N & -c_N \\ & & & & & c_N+c_{N+1} \end{bmatrix} \tag{4}$$

Here "Diag" denotes a diagonal matrix, and "Symm." denotes the symmetric part of a matrix. Applying the Laplace transform (assuming zero initial condition), the time-domain formulation can be converted to:

$$\mathbf{X}(s) = \mathbf{H}(s)\mathbf{F}(s) \tag{5}$$

where $\mathbf{H}(s)$ is known as the frequency response function (FRF) matrix and s is the complex argument. The acceleration vector in the complex domain can be expressed as:

$$\mathbf{A}(s) = s^2\mathbf{H}(s)\mathbf{F}(s) \tag{6}$$

The transmissibility function $T_{ij}(s)$ between the output DOF i and reference-output DOF j is defined as the ratio of two acceleration responses $A_i(s)$ and $A_j(s)$. Let $\mathbf{h}(s)$ denote one row of $\mathbf{H}(s)$, then

$$T_{ij}(s) = \frac{A_i(s)}{A_j(s)} = \frac{s^2\mathbf{h}_i(s)\mathbf{F}(s)}{s^2\mathbf{h}_j(s)\mathbf{F}(s)} = \frac{\mathbf{h}_i(s)\mathbf{F}(s)}{\mathbf{h}_j(s)\mathbf{F}(s)} \tag{7}$$

Consider the scenario when only one external excitation $f_k(t)$ is applied to the k-th DOF of the structure, Eq. (7) can be further simplified since the external excitation terms cancel out:

$$T_{ij}(s) = \frac{H_{ik}(s)}{H_{jk}(s)} \tag{8}$$

Thus, the transmissibility function $T_{ij}(s)$ is determined by two entries in the FRF matrix, $H_{ik}(s)$ and $H_{jk}(s)$. It is known that the transfer function matrix $\mathbf{H}(s)$ is equal to the inverse of matrix $\mathbf{B}(s)$, where

$$\mathbf{B}(s)=s^2\mathbf{M}+s\mathbf{C}+\mathbf{K}=\begin{bmatrix} m_1s^2+(c_1+c_2)s+k_1+k_2 & -c_2s-k_2 & 0 & \cdots & 0 \\ & m_2s^2+(c_2+c_3)s+k_2+k_3 & -c_3s-k_3 & \cdots & 0 \\ & & \ddots & \ddots & \vdots \\ & \text{Symm.} & & \ddots & -c_Ns-k_N \\ & & & & m_Ns^2+(c_N+c_{N+1})s+k_N+k_{N+1} \end{bmatrix} \tag{9}$$

Note that matrix **B** is a symmetric tridiagonal matrix. As a result, according to [18] which provides analytical formulation of the inverse of a tridiagonal matrix, the entries of **H**(*s*) can be expressed in a recursive form, where the complex argument "(*s*)" is neglected hereinafter to lighten the notation:

$$H_{ij}=\begin{cases} U_iU_{i+1}\cdots U_{j-1}H_{jj} & i<j \\ H_{ji} & i>j \\ [B_{ii}-X_i-Y_i]^{-1} & i=j \end{cases} \tag{10}$$

The intermediate variables U_i, X_i, Y_i are recursively computed based on entries in matrix **B(*s*)**:

$$\begin{aligned} U_i &= -[B_{ii}-Y_i]^{-1}B_{i(i+1)} && (i=1,\cdots,N-1) \\ Y_i &= \begin{cases} 0 & (i=1) \\ B_{i(i-1)}^2\,[B_{(i-1)(i-1)}-Y_{i-1}]^{-1} & (i=2,\cdots,N) \end{cases} \\ X_i &= \begin{cases} 0 & (i=N) \\ B_{i(i+1)}^2\,[B_{(i+1)(i+1)}-X_{i+1}]^{-1} & (i=1,\cdots,N-1) \end{cases} \end{aligned} \tag{11}$$

From Eq. (11), the recursive relationship between U_i and U_{i-1}can be derived as:

$$U_i=\frac{-B_{i(i+1)}}{B_{ii}+B_{i(i-1)}U_{i-1}} \qquad (i=2,...,N\text{-}1) \tag{12}$$

Eq. (12)provides the theoretical basis for the damage sensitivity analysis using transmissibility functions in this paper, where the interest is on decentralized damage detection using local excitation and local measurement. We propose to consider a decentralized damage detection approach in which acceleration measurements are taken at two neighboring DOFs at a time, following the sequence 1 and 2, 2 and 3, …, (*N*-1) and *N*. For each measurement at two neighboring DOFs, an external excitation is applied at the latter DOF in the pair. For example, the measurement is taken at DOF pair 2-3, when the excitation is applied at DOF-3. In this case, according to Eqs. (8) and (10), the transmissibility functions between each two neighboring DOFs can be expressed as:

$$T_{i(i+1)}=\frac{H_{i(i+1)}}{H_{(i+1)(i+1)}}=\frac{U_iH_{(i+1)(i+1)}}{H_{(i+1)(i+1)}}=U_i, \quad i=1,2,\cdots,N-1 \tag{13}$$

According to Eq. (11), when the complex argument *s* is large enough, U_1can be simplified as

$$U_1=\frac{-B_{12}}{B_{11}}=\frac{c_2s+k_2}{m_1s^2+(c_1+c_2)s+k_1+k_2}\approx\frac{c_2s+k_2}{m_1s^2} \tag{14}$$

Substituting Eq. (14) into Eq. (12), when *s* is large enough, U_2can be simplified as

$$U_2=\frac{-B_{23}}{B_{22}+B_{12}U_1}\approx\frac{c_3s+k_3}{m_2s^2+(c_2+c_3)s+k_2+k_3+(-c_2s-k_2)\dfrac{c_2s+k_2}{m_1s^2}}\approx\frac{c_3s+k_3}{m_2s^2} \tag{15}$$

Similarly, by iteratively applying Eq. (12), the denominator and the numerator of U_i are dominated by the term with the highest power of *s*, and U_i can be approximately expressed as

$$U_i \approx \frac{c_{i+1}s + k_{i+1}}{m_i s^2} \tag{16}$$

The equation above provides a good approximation if s has a large magnitude, i.e. at a higher frequency range, such that

$$\left|m_i s^2\right| >> \left|(c_i + c_{i+1})s\right| \text{ and } \left|m_i s^2\right| >> k_i + k_{i+1}, \quad \text{for } \forall i \tag{17}$$

To use transmissibility functions as damage indicator, the difference between the transmissibility functions of the undamaged structure and the damaged structure, ε_i, is calculated:

$$\varepsilon_i = T^D_{i(i+1)} - T_{i(i+1)} = U_i^D - U_i \tag{18}$$

where the superscript "^{D}" refers to the damaged structure. A damage indicator can be defined as the sum of the absolute value of ε_i in a certain frequency range of ω:

$$DI_i = \sum_k \left|\varepsilon_i(s_k)\right| \tag{19}$$

where $s_k = j\omega_k$ and j is the imaginary unit.

2.2 Damage scenario I – mass change

In damage scenario I, suppose that damage occurs at an arbitrary DOF n (as a reminder, the total number of DOFs is denoted by capital N), and is emulated with mass m_n (undamaged) changed to m_n^D (damage). This simple scenario is studied first because in laboratory damage detection experiments, a mass change, which affects structural dynamic properties, is often used to conveniently emulate a reversible "damage". According to Eq. (9), only one diagonal entry B_{nn} in **B** matrix will change due to the damage. Let B_{nn}^D denote the corresponding entry in **B** matrix with the changed mass. Eq. (12) indicates that after the damage, U_i will remain the same for $i < n$, and will change to U_i^D for $i \geqslant n$.

Following the local excitation and local measurement scheme (describe before Eq. (13)), the difference in transmissibility functions between damaged and undamaged structures, ε_i, can be studied in three different cases categorized by measurement locations (Figure 2). The difference can be further simplified when s is large enough (i.e. when the inequalities in Eq. (17) holds). Note the hammer icon shown in the figure is used only to represent the excitation location. In practice, the excitation record can be other types of broadband record, because the transmissibility function is independent to the excitation spectrum, as shown in Eqs. (7) and (8).

Case I (a) $i < n$

As shown in Figure 2(a) with $i < n$, acceleration measurements are taken at two neighboring DOFs i and $j = i+1$, while the external excitation is applied at DOF $j = i+1$. Eq. (12) indicates U_i will remain unchanged after damage, for $i < n$. According

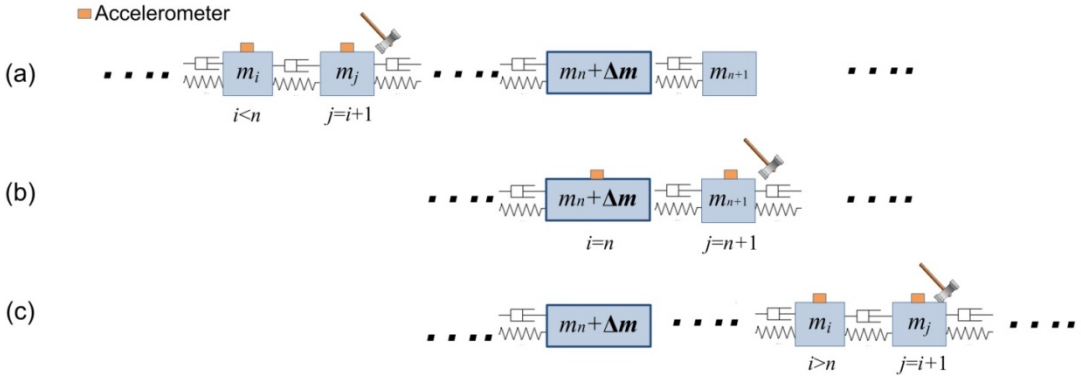

Figure 2. Damage scenario I: mass change at DOF n, while measurements are taken at DOFs i and $j=i+1$. The external excitation is applied at DOF $i+1$: (a) $i < n$; (b) $i = n$; (c) $i > n$

to Eq. (18), the transmissibility function difference ε_i equals zero in this case, i.e., the mass change at DOF *n* does not cause change in transmissibility function T_{ij} ($i < n$).

Case I (b) $i = n$

As shown in Figure 2(b), the measurements are taken at two neighboring DOFs $i = n$ and $j = n+1$, while the external excitation is applied at DOF $j = n+1$. In Eq. (12), B_{nn} is the only term that changes (to B_{nn}^D) due to the damage, and U_{n-1}will remain unchanged after damage. Substituting Eq. (12) into Eq. (18), the transmissibility function difference $\varepsilon_i = \varepsilon_n$ can be derived as:

$$\varepsilon_n = U_n^D - U_n = \frac{-B_{n(n+1)}}{B_{nn}^D + B_{n(n-1)}U_{n-1}} - \frac{-B_{n(n+1)}}{B_{nn} + B_{n(n-1)}U_{n-1}} = \frac{B_{n(n+1)}\left(B_{nn}^D - B_{nn}\right)}{\left(B_{nn}^D + B_{n(n-1)}U_{n-1}\right)\left(B_{nn} + B_{n(n-1)}U_{n-1}\right)} \tag{20}$$

Substituting Eq. (14) into the above, when *s* is large enough (satisfying inequalities in Eq. (17)), the transmissibility function difference ε_n can be simplified by neglecting lower order terms:

$$\varepsilon_n \approx \frac{-\left(c_{n+1}s + k_{n+1}\right)\left(m_n^D - m_n\right)}{m_n^D m_n s^2} \tag{21}$$

This means that unlike Case I(a), the mass change at DOF *n* causes change in transmissibility function $T_{n(n+1)}$.

Case I (c) $i > n$

As shown in Figure 2(c) with $i > n$, the measurements are taken at two neighboring DOFs *i* and $j = i+1$, while the external excitation is applied at DOF $j = i+1$. In Eq. (12), the B_{**} terms remain unchanged due to damage; only the U_{i-1} term changes to U_{i-1}^D .Substituting Eq. (12) into Eq. (18), the transmissibility function difference ε_i can be derived as:

$$\varepsilon_i = U_i^D - U_i = \frac{-B_{i(i+1)}}{B_{ii} + B_{i(i-1)}U_{i-1}^D} - \frac{-B_{i(i+1)}}{B_{ii} + B_{i(i-1)}U_{i-1}} = \frac{B_{i(i+1)}B_{i(i-1)}\varepsilon_{i-1}}{\left(B_{ii} + B_{i(i-1)}U_{i-1}^D\right)\left(B_{ii} + B_{i(i-1)}U_{i-1}\right)} \tag{22}$$

Substituting Eq. (14) into the above, when *s* is large enough (satisfying inequalities in Eq. (17)), ε_i can be simplified as:

$$\varepsilon_i \approx \frac{\left(c_i s + k_i\right)\left(c_{i+1}s + k_{i+1}\right)}{m_i^2 s^4}\varepsilon_{i-1} \tag{23}$$

According to the assumption in Eq. (17), it is easy to prove that $m_i^2 s^4 >> \left|\left(c_i s + k_i\right)\left(c_{i+1}s + k_{i+1}\right)\right|$. As a result, $|\varepsilon_i| << |\varepsilon_{i-1}|$. This means that when the measurement locations move further away from the mass change, the transmissibility function difference caused by damage reduces at a very fast rate.

To summarize all three cases with mass change, when transmissibility function T_{ij} is taken at DOFs before the excitation-measurement reaches damage location, as in Case I(a) with $i<n$, the function shows no difference between damaged and undamaged structures, i.e. $\varepsilon_i = 0$. When the transmissibility function T_{ij} is taken at locations spatially past damage, as in Case I(c) with $i>n$, the difference between transmissibility functions of damaged and undamaged structures, ε_i , is not zero but reduces very fast. Furthermore, when the transmissibility function T_{ij} is taken at DOFs after the excitation-measurement moves past damage location, as in Case I(b) with $i = n$, the difference between transmissibility functions of damaged and undamaged structures, ε_n , is significantly larger than the previous two cases. As a result, the damage indicator, DI_i, as defined in Eq. (19) and calculated for a relatively high frequency range, should be the largest when the excitation and measurements are next to the damage (Figure 2(b)). This means the damage indicator not only detects damage, but also accurately locates damage.

2.3 Damage scenario II – stiffness loss

In damage scenario II, suppose that damage occurs between DOFs n-1 and n, as the stiffness reduction from k_n to k_n^D. According to Eq. (9), only entries $B_{(n-1)(n-1)}$, $B_{(n-1)n}$, $B_{n(n-1)}$ and B_{nn} in **B** matrix will change due to the damage; all other entries remain unchanged. Let $B_{(n-1)(n-1)}^D$, $B_{(n-1)n}^D$, $B_{n(n-1)}^D$ and B_{nn}^D denote the corresponding entries in **B** matrix with stiffness loss between DOFs n-1 and n. Eq. (12) again indicates that after the damage, U_i will remain the same for $i<n$-1, and will change to U_i^D for $i \geqslant n$-1.

The difference in transmissibility functions, ε_i , can be studied into four different cases by measurement locations (Figure 3), and further simplified when s is large enough (i.e. when the inequalities in Eq. (17) holds).

Case II (a) $i < n$-1

As shown in Figure 3(a) with $i < n$-1, acceleration measurements are taken at two neighboring DOFs i and $j = i$+1, while the external excitation is applied at DOF $j = i$+1. Eq. (12) indicates U_i will remain unchanged after damage, for $i < n$-1. From Eq. (18), the transmissibility function difference ε_i equals zero in this case, i.e. the stiffness loss between DOFs n-1 and n does not cause change to transmissibility function T_{ij} ($i < n$).

Case II (b) $i = n$-1

As shown in Figure 3(b) with $i = n$-1, acceleration measurements are taken at two neighboring DOFs n-1 and n, while the external excitation is applied at DOF n. In Eq. (12), $B_{(n-1)(n-1)}$ and $B_{(n-1)n}$ are the only terms that change (to $B_{(n-1)(n-1)}^D$ and $B_{n(n-1)}^D$, respectively) due to the damage, and U_{n-2} will remain unchanged after damage. Substituting Eq. (12) into Eq. (18), the transmissibility function difference $\varepsilon_i = \varepsilon_{n-1}$ can be derived as:

$$\begin{aligned}\varepsilon_{n-1} &= U_{n-1}^D - U_{n-1} = \frac{-B_{(n-1)n}^D}{B_{(n-1)(n-1)}^D + B_{(n-1)(n-2)}U_{n-2}} - \frac{-B_{(n-1)n}}{B_{(n-1)(n-1)} + B_{(n-1)(n-2)}U_{n-2}} \\ &= \frac{B_{(n-1)n}B_{(n-1)(n-1)}^D - B_{(n-1)n}^D B_{(n-1)(n-1)} + \left(B_{(n-1)n} - B_{(n-1)n}^D\right)B_{(n-1)(n-2)}U_{n-2}}{\left(B_{(n-1)(n-1)}^D + B_{(n-1)(n-2)}U_{n-2}\right)\left(B_{(n-1)(n-1)} + B_{(n-1)(n-2)}U_{n-2}\right)}\end{aligned} \tag{24}$$

Substituting Eq. (14) into the above and neglecting lower order terms, when s is large enough, ε_{n-1} can be simplified as:

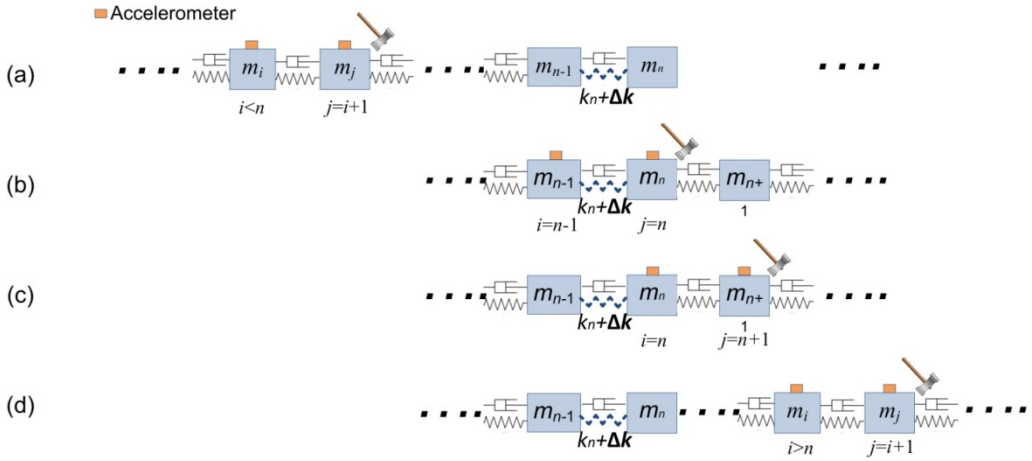

Figure 3. Damage scenario II: stiffness loss between DOFs n-1 and n, while measurements are taken at DOFs i and $j = i$+1. An external excitation is applied at DOF i+1: (a) $i < n$-1; (b) $i = n$-1; (c) $i = n$; (d) $i > n$

$$\varepsilon_{n-1} \approx \frac{(k_n^D - k_n)}{m_{n-1}s^2} \tag{25}$$

This means that unlike Case II(a), the stiffness change between DOFs *n*-1 and *n* in Case II(b) causes change in transmissibility function $T_{(n\text{-}1)n}$.

Case II (c) $i = n$

As shown in Figure 3(c) with $i = n$, acceleration measurements are taken at two neighboring DOFs *n* and *n*+1, while the external excitation is applied at DOF *n*+1. In Eq. (12), B_{nn}, $B_{n(n\text{-}1)}$ and $U_{n\text{-}1}$ are the terms that change (to B_{nn}^D, $B_{(n-1)n}^D$, and U_{n-1}^D respectively) due to the damage. Substituting Eq. (12) into Eq. (18), the transmissibility function difference $\varepsilon_i = \varepsilon_n$ can be derived as:

$$\varepsilon_n = U_n^D - U_n = \frac{-B_{n(n+1)}}{B_{nn}^D + B_{n(n-1)}^D U_{n-1}^D} - \frac{-B_{n(n+1)}}{B_{nn} + B_{n(n-1)}U_{n-1}} = \frac{B_{n(n+1)}\left(B_{nn}^D - B_{nn} + B_{n(n-1)}^D U_{n-1}^D - B_{n(n-1)}U_{n-1}\right)}{\left(B_{nn}^D + B_{n(n-1)}^D U_{n-1}^D\right)\left(B_{nn} + B_{n(n-1)}U_{n-1}\right)} \tag{26}$$

Substituting Eq. (14) into the above and neglecting lower order terms, when *s* is large enough, ε_n can be simplified as:

$$\varepsilon_n \approx \frac{-\left(c_{n+1}s + k_{n+1}\right)\left(k_n^D - k_n\right)}{m_n^2 s^4} \tag{27}$$

Comparing Eqs. (25) and (27), the relationship of transmissibility function differences for Case II (b) and Case II (c) can be derived as

$$\varepsilon_n \approx \frac{-\left(c_{n+1}s + k_{n+1}\right)m_{n-1}}{m_n^2 s^2}\varepsilon_{n-1} \tag{28}$$

Besides the assumption in Eq. (17), if we assume that the system has relatively uniform mass distribution, it is easy to prove that $|\varepsilon_n| << |\varepsilon_{n-1}|$. This means that compared with Case II(b) involving ε_{n-1}, i.e. change in transmissibility function $T_{(n\text{-}1)n}$, Case II(c) observes less change in transfer function $T_{n(n+1)}$ when *s* is large enough.

Case II (d) $i > n$

As shown in Figure 3(d), acceleration measurements are taken at two neighboring DOFs *i* and $j = i+1$, while the external excitation is applied at DOF $j = i+1$ ($i > n$). In Eq. (12), the B_{**} terms remain unchanged due to damage, and only the $U_{i\text{-}1}$ term changes to U_{i-1}^D. This situation is the same as in Case I (c) with mass change. The transmissibility function difference ε_i can be derived and simplified to be the same as in Eqs. (22) and (23) (and thus, not repeated here). As a result, this also means that when the measurement locations move further away from the stiffness change, the transmissibility function difference caused by damage reduces at a very fast rate.

To summarize all four cases with stiffness change, when transmissibility function T_{ij} is taken at DOFs before the excitation-measurement reaches damage location, as in Case II(a) with $i < n$-1, the function shows no difference between damaged and undamaged structures, i.e. $\varepsilon_i = 0$. When the transmissibility function T_{ij} is taken at DOFs after the excitation-measurement moves past damage location, as in Case II(d) with $i>n$, the difference between transmissibility functions of damaged and undamaged structures, ε_i, is not zero but reduces very fast. Furthermore, when the transmissibility function T_{ij} is taken right next to the damage, as in Case II(b) with $i = n$-1 and Case II(c) with $i = n$, the difference between transmissibility functions of damaged and undamaged structures is significantly larger than the previous two cases. Among Case II(b) and Case II(c) shown by Equation (28), the former gives larger difference between transmissibility functions of damaged and undamaged structures, i.e. $|\varepsilon_{n-1}| >> |\varepsilon_n|$ at higher-frequency domain ($s = j\omega$ has a large magnitude). Overall, the damage indicator, DI_i, as defined in Eq. (19) and calculated at a relatively high frequency range, should be the largest when the excitation and measurement are next to the damage. This means for scenarios with stiffness change, the damage indicator can also accurately locate the damage.

3. NUMERICAL SIMULATION

To validate the analytical studies in Section 2, a 10-DOF spring-mass-damper model is simulated. Table 1 summarizes the model properties of the undamaged 10-DOF spring-mass-damper model. To obtaining transmissibility functions at neighboring DOFs, the decentralized local excitation and measurement scheme described in Section 2 is strictly followed. Acceleration measurements are taken sequentially at pairs of DOFs (1-2, 2-3…, 9-10), while for each pair of measurements, an ideal impact excitation is applied at the larger DOF number. For example, acceleration measurements are taken at the 2nd and 3rd DOFs, when the excitation is applied at the 3rd DOF. The sampling rate is set to 1,000 Hz, and each measurement duration is set to 50 seconds. Using data from the undamaged structures, transmissibility functions $T_{i(i+1)}$ (i = 1, ..., 9) are calculated.

3.1 Damage scenario I –mass change

In scenario I, damage is emulated by introducing mass increase at the 6th DOF by 10%. Same as the measurement scheme of the undamaged structure, for each pair of DOFs, an ideal impact is applied at the larger DOF, and acceleration records are sequentially obtained. The transmissibility functions T_{12}^{D}, T_{23}^{D}, …, T_{9-10}^{D} for the damaged structure are calculated. Figure 4 presents the magnitude of the transmissibility functions of both the undamaged and damaged structures. For calculating the damage index in Eq. (19), the frequency range should be selected as high as possible in order to better satisfy inequalities in Eq. (17). However, in practice, the feasibility of selecting a higher frequency range is limited by many factors, such as excitation bandwidth, signal-to-noise ratio, capability of data acquisition hardware, etc. When selecting the appropriate frequency range, it is recommended to first verify the inequalities in Eq. (17) using estimated values of the structural parameters. In addition, for reliability, it is recommended to exclude frequency points close to peaks and valleys of transmissibility functions, because the transmissibility values at these points are from divisions involving very large or very small magnitude in the frequency spectra (recall that $T_{ij}(s) = A_i(s)/A_j(s)$).

Table 1. Model properties of the 10-DOF spring-mass-damper model

DOF	*Mass*	*Stiffness*	*Damping*
1~10	5.4kg (11.9 lbs)	3.44×10^4 N/m(196.67 lbs/in)	2.98 N•s/m (0.017 lbs•s/in)

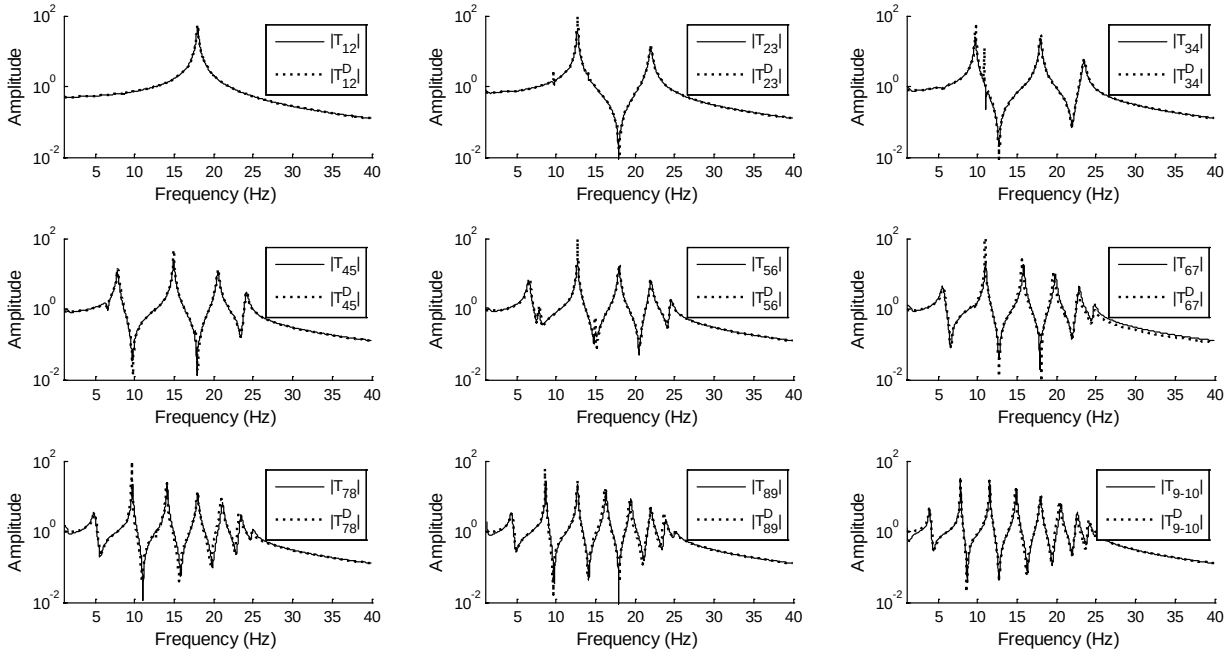

Figure 4. Comparison of transmissibility functions between undamaged and damaged structures (mass change)

To quantify the difference between transmissibility functions of damaged and undamaged structures, damage indicators DI_i are calculated based on the transmissibility function difference in frequency range 30~40Hz (Eq. (19)), and shown in Figure 5. The largest damage indicator occurs at DOFs 6-7, and other damage indicators are much smaller. This again agrees with conclusions from Section 2.2, i.e. the largest damage indicator occurs next to the mass change location. The damage indicators at other pairs of measurement locations are much smaller.

3.2 Damage scenario II – stiffness loss

In scenario II, damage is introduced by reducing the stiffness between the 6thand 7thDOFsby 10%. Again, for each pair of DOFs, an ideal impact is applied at the larger DOF, and acceleration records are sequentially obtained. The transmissibility functions T_{12}^{D} , T_{23}^{D} , …, T_{9-10}^{D} for the damaged structure are calculated. Figure 6 presents the magnitude of the transmissibility functions of both the undamaged and damaged structures. It is shown at higher frequency range, e.g.

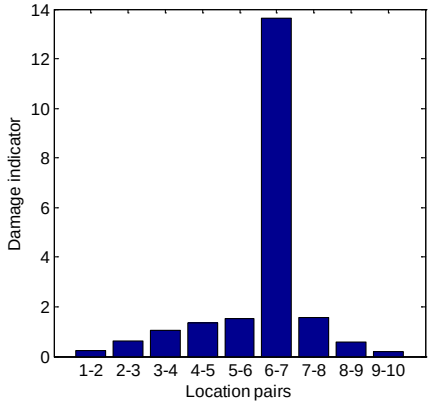

Figure 5. Damage scenario I - the damage indicators of the nine measurement pairs

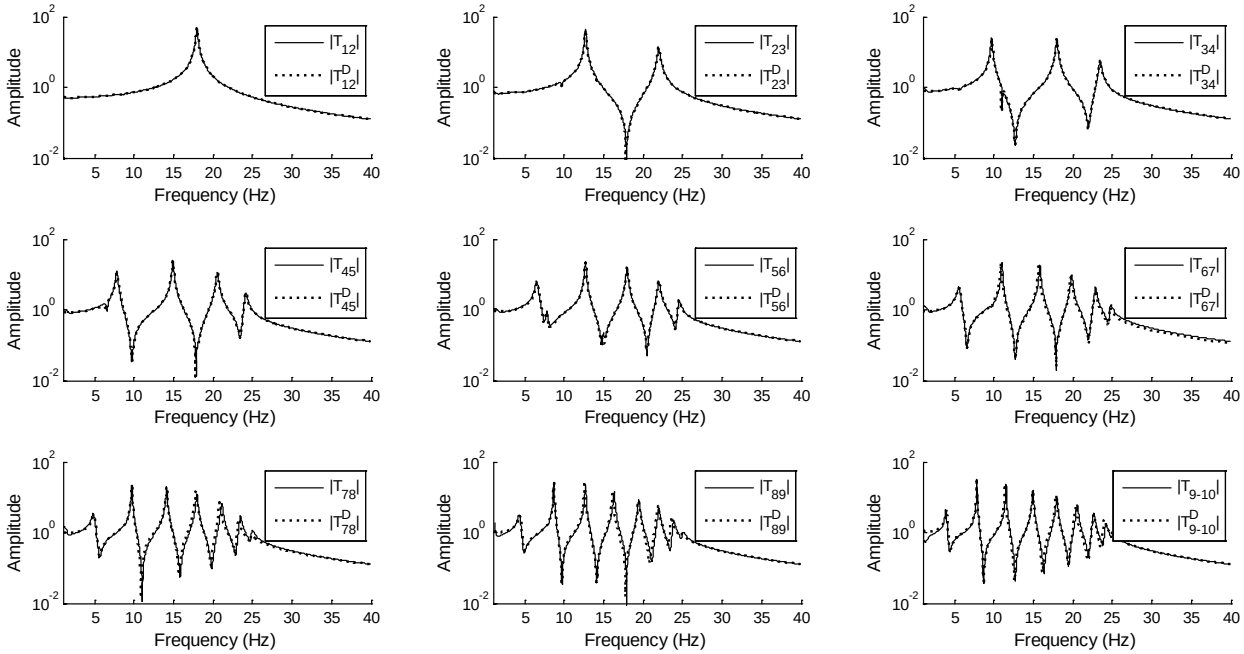

Figure 6. Comparison of transmissibility functions between undamaged and damaged structures (stiffness loss)

30~40Hz, $|T_{67}|$ (of undamaged structure) and $|T_{67}^{D}|$ (of damaged structure) have the largest difference. This agrees with the conclusions from the analytical formulation in Section 2.3.

To quantify the difference between transmissibility functions of damaged and undamaged structures, Figure 7 shows damage indicators for frequency range 30~40Hz. The largest damage indicator occurs at DOFs 6 and 7, and other damage indicators are much smaller. This again demonstrates that the largest damage indicator occurs near the damage location.

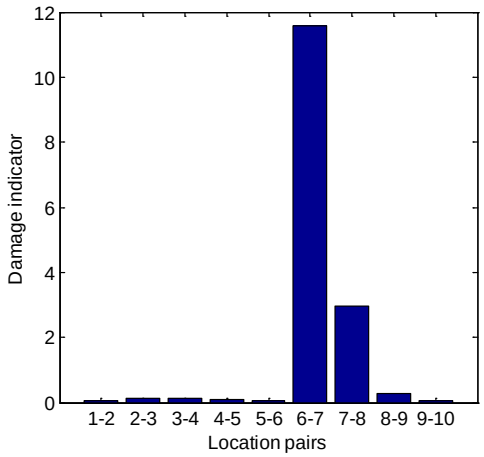

Figure 7. Damage scenario II - the damage indicators of the nine measurement location pairs (30~40Hz)

4. EXPERIMENTAL VALIDATION

To further validate the analytical studies in Section 2, a five-story shear-building structure is built for simulating a 5-DOF spring-mass-damper system. The two types of damage scenarios discussed in Section 2 are studied. The first damage scenario considers an additional mass fixed at the second floor, and the second damage scenario considers 20% stiffness loss introduced to one column between the 2nd and 3rd floors.

4.1 Testbed structure

Figure 8 shows the five-story shear-building laboratory structure. The columns are steel and the floors are aluminum. The dimension of each floor is identical: 0.41m (16 in.) long, 0.305m (12 in.) wide and 0.013m (0.5 in.) thick. The two columns have the same rectangular section, 0.15m × 0.002m (6 in. ×0.08 in.). The total height of the building is 1.524m (60 in.), with 0.305m (12 in.) per story. Each floor is connected with the columns through rigid constraints. Fixed boundary conditions are applied at the base of the each column. This five-story shear-building structure is equivalent to a 5 DOF spring-mass-damper system, because the floor stiffness is much larger than the stiffness of the columns.

Figure 8. A five-story shear-building structure

Magnet-wheeled mobile sensing nodes (MSNs), which are capable of moving on the steel structure as well as attaching/detaching an accelerometer (Silicon Designs 2260-010) onto/from structural surface, are used in the experiments. The design and implementation of the mobile sensor can be found in [19-21]. To follow the measurement scheme described in Section2, two MSNs are adopted to sequentially take measurement at each pair of floors, i.e. 1-2, 2-3, 3-4, and 4-5, as shown in Figure 9. In the experiments, when the two MSNs arrive at one pair of measurement locations, the accelerometer is attached onto the structural surface; then a hammer impact is manually applied at the higher one of the location pair to excite the structure for acceleration measurement. After the measurement, these two MSNs

detach accelerometers from structural surface, and move to next pair of measurement locations. In order to reduce the effect of experimental uncertainties, measurement at each location pair is repeatedly taken for 10 times. The sampling rate for the acceleration measurement is set as 1,000 Hz.

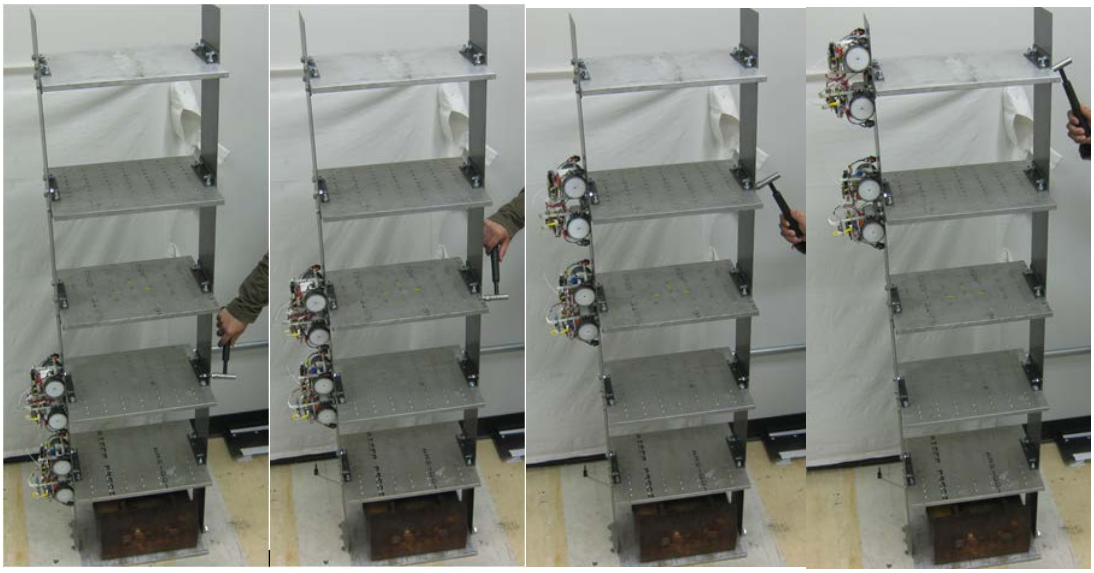

(a) Config.1 (b) Config.2 (c) Config.3 (d) Config. 4

Figure 9. Test configurations with MSNs

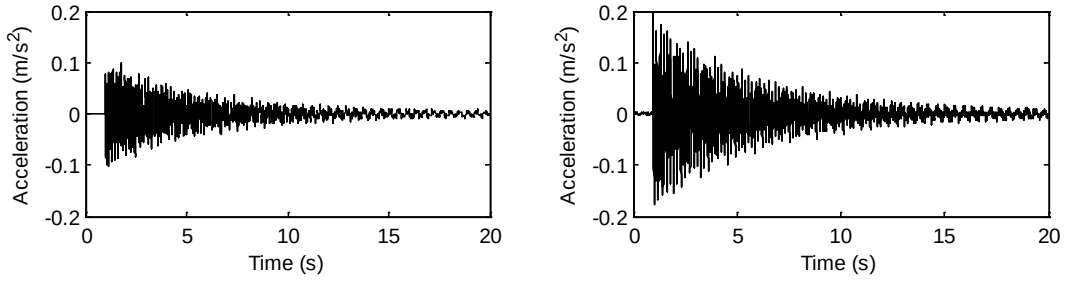

Figure 10. Example acceleration time histories when the hammer impact is applied at the 3rd floor: (a) acceleration at the 2nd floor; (b) acceleration at the 3rd floor

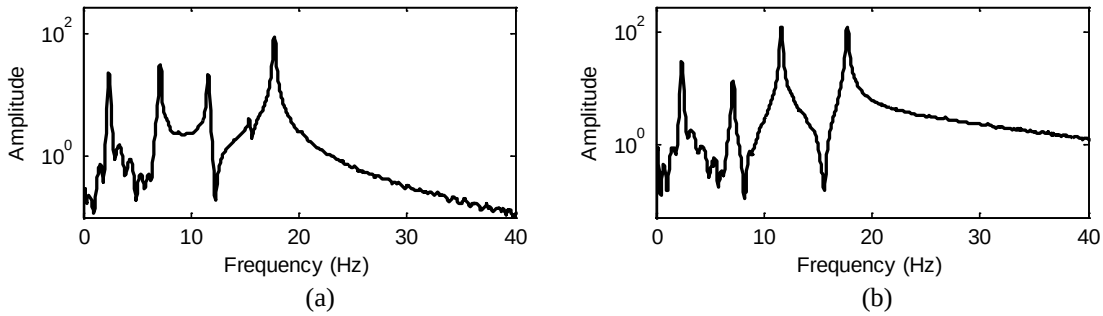

Figure 11. Example acceleration spectra when the hammer impact is applied at the 3rd floor: (a) acceleration spectra at the 2nd floor; (b) acceleration spectra at the 3rd floor

Figure 10 plots the example acceleration data at the 2nd and 3rd floors when the hammer impact is applied at the 3rd floor of the undamaged structure. Figure 11 shows the magnitude of the two frequency spectra, i.e. the discrete Fourier transform (DFT) results of the acceleration time history. According to the definition (Eq. (7)), transmissibility function T_{23} is calculated as the ratio between the two frequency spectra, as shown in Figure 12.

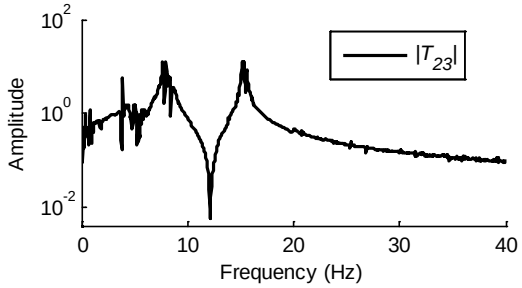

Figure 12. Transmissibility function T_{23} calculated using the example acceleration data

4.2 Damage scenario I – additional mass

In damage scenario I, a mass block of 500g (1.1 lbs) is attached on the 2nd floor (Figure 13). In contrast, the weight of each floor is about 5.025kg (11.08lbs). With the mass block attached, acceleration measurements follow the same scheme for undamaged structure.

After obtaining all the acceleration records, the transmissibility functions for the damaged structure are calculated. Figure 14 presents the magnitude of the averaged transmissibility function of both the undamaged and damaged structures. At higher frequency range, e.g. 30~40Hz, $|T_{23}|$ (of undamaged structure) and $\left|T_{23}^{D}\right|$ (of damaged structure) have the largest

Figure 13. Damage scenario I – A 500g additional mass is attached on the 2nd floor

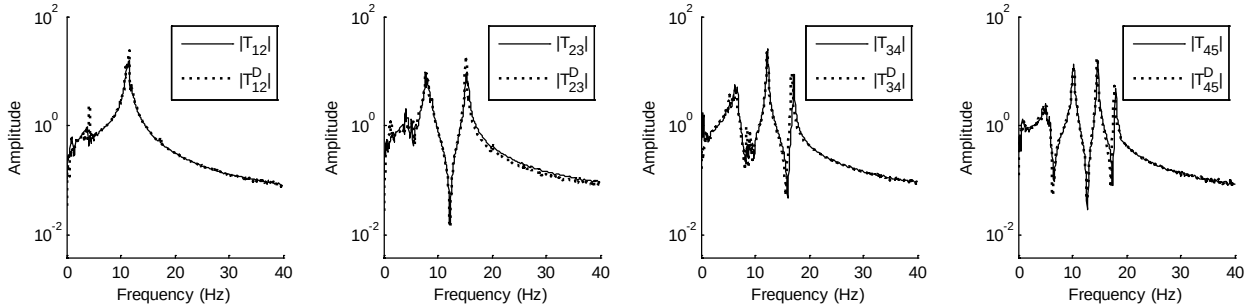

Figure 14. Comparison of averaged transmissibility function between undamaged and damaged (scenario I) structures

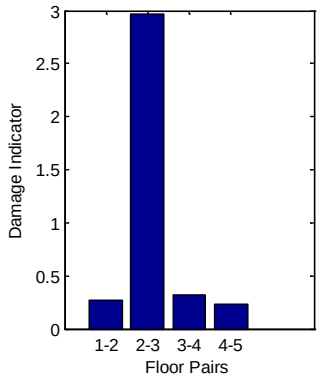

Figure 15. Damage scenario I - the damage indicators at four floor pairs (30~40Hz)

difference among all location pairs. This trend agrees with the conclusion from previous analytical derivation and numerical simulation. Figure 15 shows damage indicators for frequency range 30~40Hz. The largest damage indicator is $DI_{2\text{-}3}$, and all other damage indicators are much smaller. The experimental results confirm the effectiveness of the proposed decentralized transmissibility approach in locating damage.

4.3 Damage scenario II – stiffness loss

In damage scenario II, a 20% stiffness loss is introduced to the left column, between the 2nd and 3rd floors (Figure 16), by decreasing the section width by 20%. After the stiffness loss, acceleration measurements follow the same schemes.

Figure 16. Damage scenario II - 20% stiffness loss is introduced to the section of one column between 2nd and 3rd floors

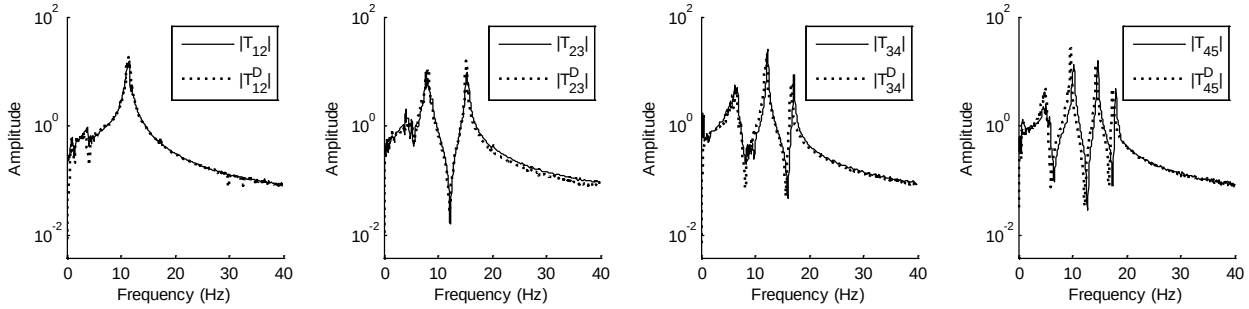

Figure 17. Comparison of averaged transmissibility function between undamaged and damaged (scenario II) structures

Figure 17 presents the magnitude of the averaged transmissibility function of both the undamaged and damaged structures. At higher frequency range, e.g. 30~40Hz, $|T_{23}|$ (of undamaged structure) and $\left|T_{23}^{D}\right|$ (of damaged structure) have the largest difference. This trend also agrees with the conclusions from two previous sections. The damage indicators are calculated based on the transmissibility function difference in frequency range 30~40Hz (Eq. (19)), and shown in Figure 18. The largest damage indicator is $DI_{2\text{-}3}$, and as expected, all other damage indicators are much smaller.

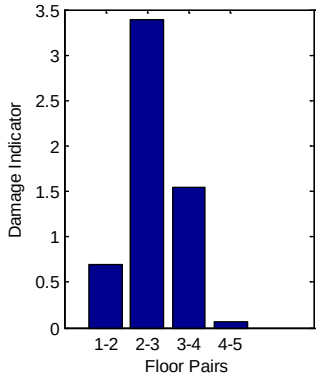

Figure 18. Damage scenario II - the damage indicators at four floor pairs

5. SUMMARY AND DISCUSSION

This study investigates the analytical nature of local transmissibility functions for decentralized damage detection, based on a chain-like multi-DOF spring-mass-damper system. Two damage scenarios are studied. The first damage scenario considers mass change, and the second damage scenario considers stiffness loss. Analytical derivations show that the difference in transmissibility functions between undamaged and damaged structures is sensitive to both damage scenarios and the largest damage indicator should occur near a damage location. The analytical derivation is validated by numerical simulations and laboratory experiments. Damage identification results in both simulations and experiments agree with the conclusion from the theoretical analysis.

The damage sensitivities of transmissibility functions have been studied on a lumped mass model in this research, using inversion of a tri-diagonal matrix. Future studies are needed for more general 2D and 3D structural models, where inversion formulation of block-diagonal matrices needs to be utilized. In addition to damage detection, future studies can also be extended to damage quantification of "hot-spot" areas, in order to facilitate structural condition assessment and retrofitting decisions. Furthermore, a mobile excitation node can also be developed to apply small-magnitude impacts, so that the decentralized measurement scheme can be automatically conducted.

ACKNOWLEDGEMENT

This research was partially funded by the National Science Foundation (CMMI-1150700 and CMMI-1041607) and the Georgia Department of Transportation (RP12-21). Any opinions, findings, and conclusions or recommendations expressed in this publication are those of the author and do not necessarily reflect the view of the sponsors.

REFERENCES

[1] ASCE, *Report Card for America's Infrastructure*. Reston, VA: American Society of Civil Engineers, 2013.

[2] J. M. Ko and Y. Q. Ni, "Technology developments in structural health monitoring of large-scale bridges," *Engineering Structures*, vol. 27, pp. 1715-1725, 2005.

[3] C. R. Farrar, H. Sohn, F. M. Hemez, M. C. Anderson, M. T. Bement, P. J. Cornwell, S. W. Doebling, J. F. Schultze, N. Lieven, and A. N. Robertson, *Damage Prognosis: Current Status and Future Needs*, Los Alamos National Laboratory, Los Alamos, NM, LA-14051-MS, 2003.

[4] M. Çelebi, *Seismic Instrumentation of Buildings (with Emphasis on Federal Buildings)*, United States Geological Survey, Menlo Park, CA, 0-7460-68170, 2002.

[5] S. W. Doebling, C. R. Farrar, and M. B. Prime, "A summary review of vibration-based damage identification methods," *The Shock and Vibration Digest*, vol. 30, pp. 91-105, 1998.

[6] W. Fan and P. Z. Qiao, "Vibration-based damage identification methods: a review and comparative study," *Structural Health Monitoring-an International Journal*, vol. 10, pp. 83-111, 2011.

[7] H. Y. Li and H. Xu, "Damage detection for structural health monitoring using ultrasonic guided waves," in *Advances in Fracture and Damage Mechanics Xi*. vol. 525-526, Q. F. Li, Y. L. Li, and M. H. Aliabadi, Eds., 2013, pp. 433-436.

[8] H. Uchida, L. Brigatti, and J. Caprioli, "Detection of structural damage from glaucoma with confocal laser image analysis," *Investigative Ophthalmology & Visual Science*, vol. 37, pp. 2393-2401, 1996.

[9] C. Colla, P. C. Das, D. McCann, and M. C. Forde, "Sonic, electromagnetic and impulse radar investigation of stone masonry bridges," *Ndt & E International*, vol. 30, pp. 249-254, 1997.

[10] C. Cheng and M. Sansalone, "The Impact-echo response of concrete plates containing delaminations - numerical, experimental and field studies," *Materials and Structures*, vol. 26, pp. 274-285, 1993.

[11] T. K. Lin, S. L. Hung, and C. S. Huang, "Detection of damage location using a novel substructure-based frequency response function approach with a wireless sensing system," *International Journal of Structural Stability and Dynamics*, vol. 12, 2012.

[12] A. Sadhu and S. Narasimhan, "A decentralized blind source separation algorithm for ambient modal identification in the presence of narrowband disturbances," *Structural Control and Health Monitoring*, vol. 21, pp. 282-302, 2014.

[13] H. Zhang, M. J. Schulz, F. Ferguson, and P. F. Pai, "Structural health monitoring using transmittance functions," *Mechanical Systems and Signal Processing*, vol. 13, pp. 765-787, 1999.

[14] H. R. Kess and D. E. Adams, "Investigation of operational and environmental variability effects on damage detection algorithms in a woven composite plate," *Mechanical Systems and Signal Processing*, vol. 21, pp. 2394-2405, 2007.

[15] C. Devriendt and P. Guillaume, "Identification of modal parameters from transmissibility measurements," *Journal of Sound and Vibration*, vol. 314, pp. 343-356, 2008.

[16] Z. Mao and M. Todd, "A model for quantifying uncertainty in the estimation of noise-contaminated measurements of transmissibility," *Mechanical Systems and Signal Processing*, vol. 28, pp. 470-481, 2012.

[17] T. J. Johnson and D. E. Adams, "Transmissibility as a differential indicator of structural damage," *Journal of Vibration and Acoustics-Transactions of the ASME*, vol. 124, pp. 634-641, 2002.

[18] E. M. Godfrin, "A method to compute the inverse of an N-block tridiagonal quasi-Hermitian matrix " *Journal of Physics-Condensed Matter*, vol. 3, pp. 7843-7848, 1991.

[19] D. Zhu, X. Yi, Y. Wang, K.-M. Lee, and J. Guo, "A mobile sensing system for structural health monitoring: design and validation," *Smart Materials and Structures*, vol. 19, p. 055011, 2010.

[20] J. Guo, K.-M. Lee, D. Zhu, X. Yi, and Y. Wang, "Large-deformation analysis and experimental validation of a flexure-based mobile sensor node," *IEEE/ASME Transactions on Mechatronics*, vol. 17, pp. 606-616, 2011.

[21] D. Zhu, J. Guo, C. Cho, Y. Wang, and K.-M. Lee, "Wireless mobile sensor network for the system identification of a space frame bridge," *IEEE-ASME Transactions on Mechatronics*, vol. 17, pp. 499-507, 2012.